Qinghui Liu et al.: Observation of Atmospheric Disturbances Using a Real-Time VLBI System, IVS 2002 General Meeting Proceedings, p.147–151
http://ivscc.gsfc.nasa.gov/publications/gm2002/liu

Observation of Atmospheric Disturbances Using a Real-Time VLBI System

Qinghui Liu [1], *Masanori Nishio* [2], *Kunihiro Yamamura* [1], *Tomoyuki Miyazaki* [1]

[1)] *Department of Electrical and Electronics Engineering, Kagoshima University*

[2)] *Department of Physics, Kagoshima University*

Contact author: Qinghui Liu, e-mail: eem0338@elib.eee.kagoshima-u.ac.jp

Abstract

This paper reports observation results of atmospheric disturbances on a very long baseline. Using a real-time VLBI system, the observation was performed by the Kagoshima 6-m and the Mizusawa 10-m radio telescopes, which are 1,284 km apart. Beacon waves from geostationary satellites were received and data were sent via public communication lines. The time variation of the correlation phase obtained was analyzed by calculating the Allan standard deviation, $\sigma_y(\tau)$ and the time structure function, $D_\phi(\tau)$, as a function of a time interval τ. It is found that the time variations of the correlation phase were mainly caused by atmospheric disturbances, and that for 1 s$< \tau <$ 200 s, the Allan standard deviation of atmospheric disturbances $\sigma_y(\tau) \propto \tau^{-0.2}$ and the time structure function $D_\phi(\tau) \propto \tau^{5/3}$.

1. Introduction

Atmospheric disturbances, which are mainly caused by fluctuations of water vapor distribution in the troposphere, bring about phase fluctuations of radio waves passing through the troposphere. In VLBI, the phase fluctuations not only decrease the angular resolution, but also cause coherence loss.

Observations of atmospheric disturbances were made with a real-time VLBI system developed for diagnosis of VLBI observation facilities [1]. In this paper, observation results are reported.

2. Real-time VLBI System

The block diagram of the real-time VLBI system is shown in Fig.1. The system consists of two remotely located antennas connected with data transmission lines using ISDN and a PC-based cross-correlator. In the system, beacon waves of 19 GHz emitted from geostationary satellites are received by the two antennas. The signals received are recorded into PCs after down-conversion and 2-bit A–D conversion. Bandwidth of the signals is ten-odd kilohertz. Local signals for the down-conversion and clocks for the A–D conversion are supplied by hydrogen maser oscillators. The time synchronization is made by recording 1-pps signals together with the A–D converted signals. In addition, start of the A–D conversion is synchronized with the 1-pps signals. An accuracy of an order of 1 μs is achieved in the time synchronization between two recorded signals.

The signal received by the antenna located at a remote station (Y-Station in Fig. 1) is transmitted to a personal computer PC_Z located at another station (X-Station in Fig. 1) at a rate of 128 kbps by FTP. On the other hand, the signal received by the antenna located at X-station is transmitted to PC_Z via Ethernet. Cross-correlation between the two signals is calculated with PC_Z.

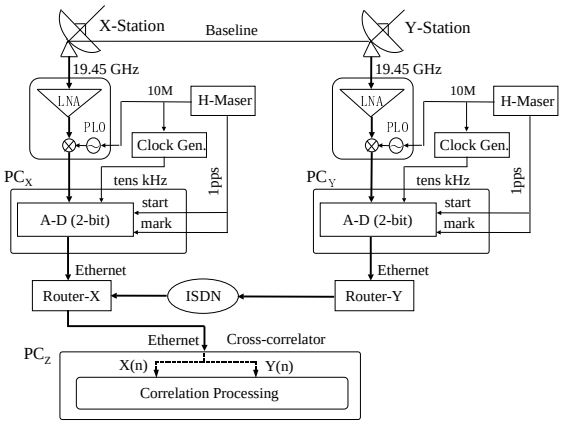

Figure 1. Block diagram of the real-time VLBI system.

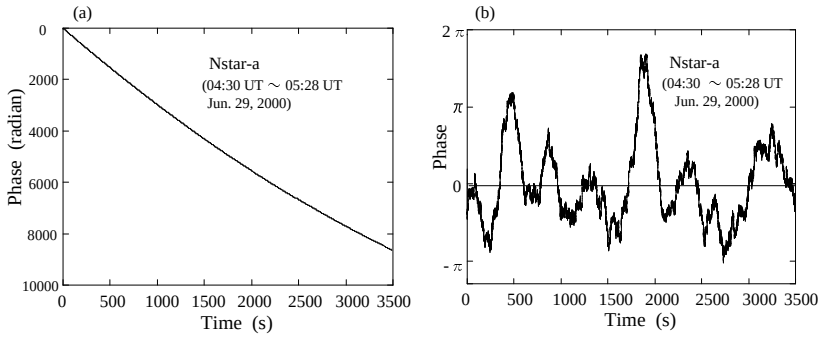

Figure 2. Correlation phase. (a) before fringe stopping and (b) after fringe stopping.

The correlation phase shows temporal variations caused by atmospheric disturbances overlaid on a gradual variation by the orbital motion of the satellite. The latter component, $\phi_s(t)$ is calculated from the observed phase variations by the method of least squares with a period, T_p. In the next step, the fringe stopping was carried out by which the component, $\phi_s(t)$ is subtracted from the time variations of the correlation phase observed.

3. Observations and Results

Observations of atmospheric disturbances were made using the Kagoshima 6-m and the Mizusawa 10-m radio telescopes. The baseline length is 1,284 km. Two geostationary satellites, Nstar-a and Nstar-b, are used for the observations. The frequencies of the beacon waves are 19.45 GHz. Nstar-a was observed twice from 04:30 to 05:28 UT on June 29, 2000 and from 00:00 to 00:57 UT on June 30, 2000. Furthermore, Nstar-b was observed three times: 05:40–06:17 UT on June 29, 2000, 07:30–08:15 UT on June 29, 2000, and 01:10–02:07 UT on June 30, 2000.

The received bandwidth was 12.5 kHz, and the sampling frequency was set at 25 kHz. The data

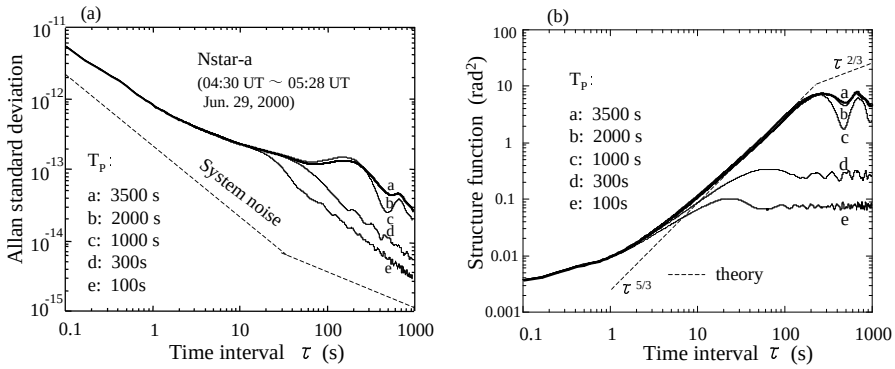

Figure 3. (a) Allan standard deviation and (b) time structure function with different values of $T_{\rm p}$.

at the Mizusawa station were transmitted to the Kagoshima station via ISDN. At the Kagoshima station, the correlation phase was calculated with an integration time of 82 ms.

Figure 2(a) shows the correlation phase before fringe stopping for the data from 04:30 UT to 05:28 UT on June 29, 2000. As shown in Fig. 2(a), the correlation phase decreased monotonically. By the method of least squares with $T_{\rm p}$=3,500 s, the following expression for the component of long period of the correlation phase was obtained:

$$\phi_{\rm s}(t) = 2.0181 \times 10^{-4} t^2 - 3.1684t, \tag{1}$$

where t is measured in second. It was confirmed that the coefficients of each term in $\phi_{\rm s}$ agreed with those calculated from the orbital data of the satellite. The correlation phase after fringe stopping using Eq. (1) is shown in Fig. 2(b).

4. Analysis

In order to analyze the time variation of the correlation phase $\phi(t)$, the Allan standard deviation, $\sigma_y(\tau)$ [2], and the time structure function, $D_\phi(\tau)$ [3], were calculated;

$$\sigma_y(\tau) = \frac{1}{\sqrt{2}\omega\tau}\langle[\phi(t+2\tau) - 2\phi(t+\tau) + \phi(t)]^2\rangle^{1/2} \tag{2}$$

$$D_\phi(\tau) = \langle[\phi(t+\tau) - \phi(t)]^2\rangle \tag{3}$$

Here, ω is the observation angular frequency, τ is a time interval, and $\langle\cdot\rangle$ means time averaging.

Figures 3(a) and 3(b) show the Allan standard deviations and the time structure functions of the correlation phase variation for different values of $T_{\rm p}$, respectively. The dashed line in Fig. 3(a) is the calculated result of $\sigma_y(\tau)$ of the system noise including the instability of hydrogen maser oscillators, thermal noise, and so on. The dashed line in Fig. 3(b) is the theoretical curve of $D_\phi(\tau)$ of atmospheric disturbances [3]. As seen in Fig. 3(a), the magnitude of $\sigma_y(\tau)$ of the time variations of the correlation phase observed was three times larger than that of the system noise. Thus, the main cause of the time variation of the correlation phase observed is considered to be atmospheric disturbances.

For $T_{\rm p} > 1,000$ s, the curves of $\sigma_y(\tau)$ almost did not depend on $T_{\rm p}$ for the entire region of τ, and showed a flat region for $\tau < 200$ s. On the other hand, the time structure functions showed the

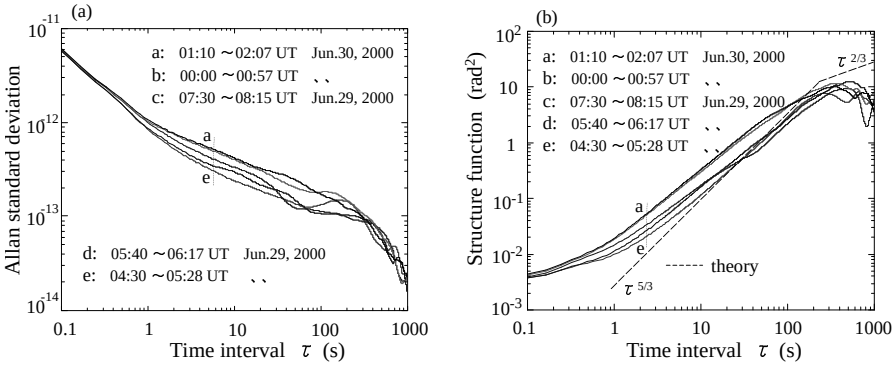

Figure 4. (a) Allan standard deviation and (b) time structure function of the 5 observations.

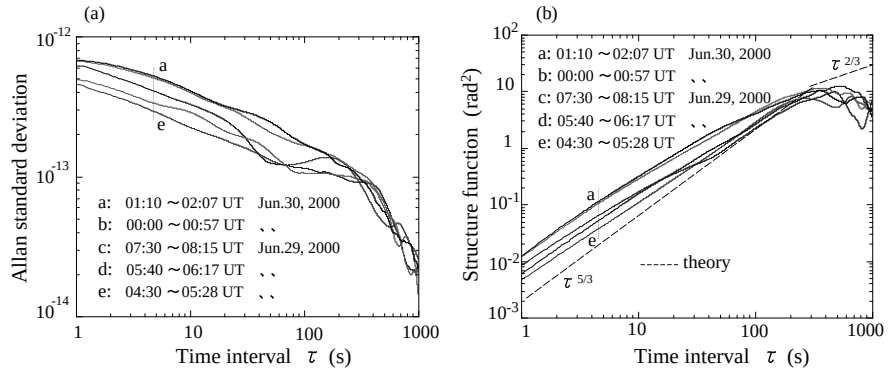

Figure 5. (a) Allan standard deviation and (b) time structure function of the 5 observations after moving-averaging with T_a=1 s.

independence of T_p, and approached the theoretical curve, $D_\phi(\tau) \propto \tau^{5/3}$ in the region of $\tau < 200$ s [3]. That is to say, to get the information of atmospheric disturbances with long period, T_p is required to be longer than 1,000 s.

Figure 4(a) shows the Allan standard deviations and Figure 4(b) shows the time structure functions of the time variations of the correlation phase observed in this work. The values of T_p were different for different observations, but larger than 2,000 s. As seen in Fig. 4(a) and 4(b), for τ <1 s, the curves of the five observations coincide with each other for either $\sigma_y(\tau)$ or $D_\phi(\tau)$. In this region, $\sigma_y(\tau) \propto \tau^{-0.8}$ and $D_\phi(\tau)$ does not change so much compared with that in other regions except for $\tau > 200$ s. These facts suggest that the dominant factor of the correlation phase variations in the region is white phase noise.

In the next step, the component of high frequency in the time variations of the correlation phase was subtracted by the moving average method with an interval T_a=1 s. Figures 5(a) and 5(b) show the results for the moving-averaged time variations of the correlation phase. As seen in Fig. 5, in the region of 1 s< τ <200 s, the curves are almost parallel to each other and $\sigma_y(\tau) \propto \tau^{-0.2}$, and $D_\phi(\tau) \propto \tau^{5/3}$. These facts suggest that the dominant factor of the correlation phase variations in the region is flicker frequency noise. On the other hand, in the region of τ >200 s, where

$\sigma_y(\tau) \propto \tau^{-1}$, the main factor of the correlation phase variations seems to be white phase noise.

5. Discussion

The explanation of the results obtained in this work was made with a frozen-screen model of atmospheric disturbances [4]. In the model, water vapor is contained in tropospheric screens of various sizes, which move horizontally over the antennas at an average velocity. In each screen, the distribution of water vapor is given by Kolmogorov's turbulence theory. The motion of the screens and the turbulence inside the screens cause random variations in the phase of radio waves passing through the screens.

The quick variation of the correlation phase in the region of $\tau < 1$ s may be mainly caused by turbulence inside the screens. The coincidence of the curves of the five observations suggests that the strength of the turbulence inside the screens varied slightly during the observation time.

The correlation phase variation in the region of 1 s$< \tau <$200 s may be mainly caused by the motion of the screens. The variations of $\sigma_y(\tau)$ and $D_\phi(\tau)$ in this region reflect the strength of atmospheric disturbances.

The profile of $\sigma_y(\tau)$ and $D_\phi(\tau)$ for $\tau > 200$ s mainly reflects to the phase variations with large amplitude and period longer than several hundred seconds, which may be mainly caused by the motion of large screens. Since the observation periods in this work were less than 1 hour, we could not exactly confirm the properties of $\sigma_y(\tau)$ and $D_\phi(\tau)$ for $\tau >$200 s. We will get data for longer observation time to study the properties of $\sigma_y(\tau)$ and $D_\phi(\tau)$ for τ larger than several hundred seconds.

6. Conclusions

For real-time observations of atmospheric disturbances on a very long baseline, the beacon waves of the geostationary satellites were received using the Kagoshima 6-m and the Mizusawa 10-m radio telescopes. From the Allan standard deviation and the time structure function, it is found that the time variations of the correlation phase were mainly caused by atmospheric disturbances, and that for 1 s$< \tau <$ 200 s, the Allan standard deviation of atmospheric disturbances $\sigma_y(\tau) \propto \tau^{-0.2}$ and the time structure function $D_\phi(\tau) \propto \tau^{5/3}$. The profiles of $\sigma_y(\tau)$ and $D_\phi(\tau)$ were explained with a frozen-screen model of atmospheric disturbances.

References

[1] M. Nishio, Q. Liu, T. Miyazaki, N. Kawaguchi, T. Sasao, T. Omadaka, and M. Morimoto, "Development of real-time diagnostic system for VLBI using public communication lines," IEICE Trans.B(in Japanese), vol.J83–B, no.8, pp.1195–1202, 2000; Electronics and Communications in Japan, John Wiley & Sons, part 2, vol.84, no.6, pp.1–9, 2001.

[2] A.E.E Rogers and J.M. Moran, "Coherence limits for very long baseline interferometry," IEEE trans., Instrum. & Meas., IM–30, no.4, pp.283–286, 1981.

[3] A.F. Dravskikh and A.M. Finkelstein,"Tropospheric limitations in phase and frequency coordinate measurement in astronomy," Astrophys. Space Sci., vol.60, pp.251–265, 1979.

[4] C.R. Masson,"Atmospheric effects and calibration in astronomy with millimeter and submillimeter wave interferometry," M. Ishiguro and W.J. Welch, Eds., Astron. Soc. Pacific Conf. Series 59, pp.87–95, 1994.